# Numerical Investigation of the Heat Transfer in a Meandering Millichannel by a coupled 1D-Flow-Channel / 3D-Surrounding-Solid Model

Antoinette Maarawi, Zoé Anxionnaz-Minvielle, Pierre Coste, Nathalie Di Miceli Raimondi, Michel Cabassud

# Numerical Investigation of the Heat Transfer in a Meandering Millichannel by a coupled 1D-Flow-Channel / 3D-Surrounding-Solid Model

Antoinette Maarawi [a], Zoé Anxionnaz-Minvielle [a]*, Pierre Coste [a], Nathalie Di Miceli Raimondi [b], Michel Cabassud [b]

a Univ. Grenoble Alpes, CEA, LITEN, DTCH, Laboratoire Composants et Systèmes Thermiques, 38000 Grenoble, France
b Laboratoire de Génie Chimique, Université de Toulouse, CNRS, INPT, UPS, Toulouse, France
*zoe.minvielle@cea.fr

Heat exchanger/reactors with corrugated channels are used to implement especially exothermal chemical reactions. Heat conduction effects in their solid material are not negligible and induce in particular heat flows between adjacent channels. In this context, this work proposes a model of a plate-type heat exchanger/reactor with a 2D-meandering millichannel, taking into account these conduction effects by coupling a 1D approach for the channel flow, with correlations for the friction factor and the Nusselt number, to a 3D approach for the solid part. This model is a compromise between the 1D classical reactor models that don't account for 3D conduction effects in the solid and the 3D simulations of the channel flow with the surrounding solid which are computationnally expensive or unachievable for a large reactor. In the tested case, the 1D/3D and 3D CFD results are in good agreement (5 min vs 4 h computational time), which suggests valid model assumptions and internal model consistency. Simulated and experimental conversion rates of a fast highly exothermic reaction are then compared, showing the relevancy of the model. Further investigations are performed to highlight the effect of conjugate heat transfer in millistructured heat exchangers and to quantify its limitations versus the 1D/3D model.

**Keywords:** heat exchanger/reactor; modelling; heat transfer; exothermic reaction; process intensification; corrugated channel

## 1. INTRODUCTION

Process intensification has been defined in several ways in the literature [1]–[3]. However, all the definitions focus on the multidisciplinary nature of this engineering approach with the goal of developing innovative technologies that offer processes that are more environmentally friendly and energy efficient, as well as processes that are more productive and operate safely. Process intensification may lead to design multifunctional and compact units such as compact heat exchangers/reactors. The combination of two unit operations in the same miniaturised apparatus (heat exchange and reaction) enables process intensification. Different kinds of compact heat exchangers/reactors (HEX reactors) exist and are summarized in the review of Anxionnaz et al. [4]. They are promising for the implementation of chemical syntheses, especially fast and exothermic ones, by offering efficient heat and mass transfer and temperature control. However, carrying out chemical reactions requires a

sufficient residence time for the chemistry. Fluid velocities are though moderate, resulting in laminar to transitional flow regime conditions in miniaturised reactors. Therefore, in order to maintain a plug flow and intensify heat and mass transfer, generating vorticity in the flow regions is a key success factor. This can be achieved using several methods that exist in the literature, such as jets [5] and turbulence promoters or vorticity generators for generating embedded vortices [6], [7], and wall curvature [8]–[10] for inducing secondary flows (Dean vortices). This last technique leads to implementing corrugated geometries in compact HEX reactors. Plate HEX reactors with wavy channels exist in the literature and are commonly used due to their compactness and modularity regarding the number of plates. Examples for such devices are the LFR and AFR from Corning [11], the Marbond from Chart Martson [12], the Flow Plate from Lonza and Ehrfeld Mikrotechnik [13], the OPR from Alfa Laval Vicarb [14], the MR500 from 3M Technical Ceramics [15], the ART plate reactor PR37 from Ehrfeld Mikrotechnik GmbH [9] and the DeanHex from the Laboratoire de Génie Chimique (LGC, France) and the Commissariat à l'Energie Atomique et aux Energies Alternatives (CEA, France) [8]. Their corrugated geometry allows the generation of secondary motions (i.e. Dean vortices), that are responsible for flow mixing and heat and mass transfer enhancement. Therefore, these micro/millistructured heat exchanger/reactors are preferably used to conduct highly exothermic reactions that cannot be carried out in a batch reactor without high risk of thermal runaway.

The present work focuses on the "DeanHex" plate HEX reactor that consists of a stack of process plates (where the reaction takes place) and utility plates (for cooling or heating), where millichannels are engraved by laser machining (cf. Figure 1).

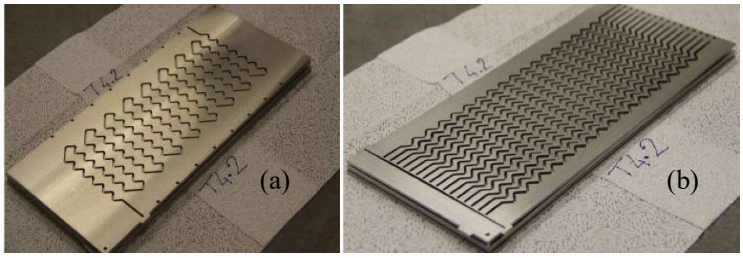


*Figure 1: DeanHex heat exchanger/reactor pilot: (a) process plate and (b) utility plate [16].*

Experiments conducted on the "DeanHex" reactor showed a shift to a lower Reynolds number (equal to 200) of the transition between laminar and turbulent flow compared to straight channels thanks to the corrugation of the reaction channel [8], [16]. Heat and mass transfers are thus intensified and plug flow behaviours are obtained while working under flow conditions that usually lead to laminar flow regime. The number of plates is dependent on the application, in order to provide the required residence time to complete the chemistry. The geometry of the reaction channel consists of periodic zigzag units and is represented in Figure 2. In this work, a square process channel with a hydraulic diameter $d_h$ of 2 mm, a radius of curvature of the bends $R_c$ of 1.5 mm, a 7 mm long straight section $L_s$ between two bends and an angle θ between two straight sections equal to 90 °, is considered.

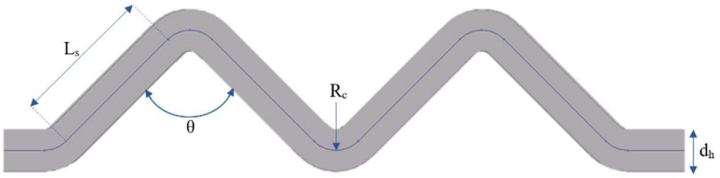


*Figure 2: Schematic of the zigzag channel with geometric parameters [17].*

Even if the use of micro/millistructured heat exchanger/reactors is an interesting alternative to "batch" systems, the number of parameters to consider for their design (hydrodynamics, heat and mass transfer, etc.) makes it difficult to scale them up to industrial scale. In this context, numerical simulation is a useful tool to study the system and analyse the influence of channel dimensions on the flow during the scale-up process.

Since the flow in micro- and millichannels is of the plug flow type, classical 1D models based on the same assumptions as those used for modelling conventional continuous reactors can be developed [18]. However, these models do not generally consider all the heat conduction effects in the solid material which are not negligible in micro- and millistructured heat exchangers/reactors (high solid/fluid volume ratio) and induce in particular heat flows between adjacent channels. Indeed, in these intensified devices (cf. Figure 1), the "process" channel meanders through the "process" plate to give the sufficient fluid residence time. The conductive materials used and the proximity of the adjacent channels because of compactness mean that there are heat flows between these channels, not only between the "process" channel and the "utility" channel. In order to increase the compactness of heat exchangers/reactors, the distance between adjacent channels is decreased, reducing the thermal resistance due to the walls. Heat is not only transported from one fluid perpendicularly through the wall to the other fluid, but mainly in all directions (three-dimensional heat flow). This represents the so-called "conjugate heat transfer" and must be taken into account, especially in micro/millistructured compact devices. Boundary conditions such as a constant temperature on the channel wall or a constant heat flux on the wall no longer apply and the heat transfer in the solid-fluid system must be calculated simultaneously with the flow field [19], [20]. To our knowledge, there is only one 1D modelling work that has addressed these conduction effects, in which a model for the PR37 plate ART heat exchanger/reactor designed by Ehrfeld Mikrotechnik GmbH was developed [19]. This model consists in calculating the heat flow between a given position in the process channel and all sections of the utility channel using a thermal resistance network. The only adjustable parameters of the model are the parameters of the Nusselt correlations used to calculate the heat transfer resistances in the channels. According to the authors, this model allows to simulate the heat transfer in the reactor with few computational resources and with high accuracy over a wide range of operating conditions.

Furthermore, throughout the years, three-dimensional (3D) CFD simulations have been conducted for corrugated micro- and millichannels, for a better representation of the local physico-chemical phenomena. However, Table 1 shows that the simulated domain, in several heat transfer numerical studies from the literature, carried out for other corrugated channels than the DeanHex, consists of "only" one to a few periodic units to minimize the computational time and resources. Nevertheless, the number of mesh elements required to conduct the simulations is still high, making the simulations long and complex. In fact, the complex geometries of the channels (especially the presence of bends) with a high $L/d_h$ ratio and the large number of units which may not be all periodic (cf. Figure 1) would make 3D CFD simulations highly demanding in staff and computational resources.

| References | Year of the simulation | Number of simulated periodic units | Total number of computational volume elements |
|---|---|---|---|
| Facão and Oliveira[25] | 2005 | 1 | 833 000 |
| Rosaguti et al.[22] | 2007 | 1 | 210 000 |
| Sui et al. [26] | 2012 | 1 | 136 653 |
| Zheng et al.[23] | 2013 | 10 | 10 000 000 |
| Zheng et al.[24] | 2013 | 14 | 13 000 000 |
| Karale et al.[27] | 2013 | 1 | 450 000 |
| Abed et al.[28] | 2015 | 10 | 2 340 000 |
| Premkumar D et al.[21] | 2016 | 3 | 2 030 188 |

*Table 1: Simulated domains and number of mesh elements used in 3D CFD simulations of corrugated channels.*

For the "DeanHex" reactor, 3D CFD simulations of 3 to 11 periodic units (depending on the case) of the heat transfer in the square zigzag millichannels has been carried out in the recent study of Shi et al. [29]. The simulations were conducted in stationary laminar flow conditions, using the finite volume CFD code, ANSYS CFX 16. Several channel geometries ($L_s$=2-12 mm) with a total length of 0.1 m were modelled. In terms of meshing, respectively 4.3 million (at Re=224) and 7.6 million (at Re=560) mesh elements were needed for the wavy channels consisting of 8 and 4 periodic units.

Consequently, for the purposes of rapid simulations of case studies and of building a general model for the millistructured heat exchanger/reactor (DeanHex) that is able to predict the performance of this device in different applications and at scales up to the industrial one, this work deals with an 1D/3D numerical appoach which aims at:

- in comparison with the 1D classical approaches of reactor modelling: taking into account the thermal conduction effects in the solid material which are not negligible in the DeanHex (high solid volume to fluid volume ratio) and induce, in particular, heat transfer between adjacent

channels; and providing a finer representation of the heat transfer process, with local heat transfer coefficients from wall to fluid used in the simulations;

- in comparison with the 3D CFD simulations: providing a less resource demanding simulation tool for millichannel geometry with a high $L/d_h$ ratio.

The full description of this approach is detailed in a previous work [17]. In the present work, the validation of the model is addressed in two parts: first with 3D CFD simulations and then with previous experimental works conducted in the "DeanHex" zigzag millichannel with a fast and exothermic chemical reaction. In each part, a comparison of results is made in order to discuss the relevance and the accuracy of the proposed model.

## 2. NUMERICAL APPROACH

### 2.1 Principle

The 1D/3D numerical approach [17] used in the present work consists in representing the meandering flow channel by a 1D model coupled to a 3D model for the surrounding solid in which the channel is embedded. The 1D model considers all process variables but with reduced calculation time compared to 3D approaches, which are generally focused on local effects. In the 1D model, calculated variables are averaged over the cross-sections of the channel and discretised along the channel; heat is exchanged in all normal directions to its walls with the surrounding solid. Correlations, related to thermal performance and friction laws for example, that have been obtained during experimental works are integrated in this 1D model. Correlations may also be obtained with a validated 3D CFD approach on a limited number of periodic units. The 1D model is coupled to a 3D model for the surrounding solid in order to take into account the thermal conduction effects in the heat transfer process simulation. Consequently, this approach not only avoids meshing the channel cross-section with a complex 3D mesh, but also provides a simulation method capable of predicting the performance of the heat exchanger/reactor (conversion rate, selectivity, etc...). It intends to bridge the gap between the simulation at small scale and the simulation at the reactor scale, at a reasonable CPU cost. The numerical resolution of this 1D/3D model is performed using COMSOL Multiphysics V5.5.

### 2.2 Computational domain

The three-dimensional zigzag channel is represented by a one-dimensional curve "C" following the axial direction of the flow in the channel. The channel is embedded in a solid matrix to form the reactor; thus in the COMSOL model, "C" is surrounded by the 3D solid "S". However, doing so, the geometry of the solid is not well represented which will lead to the application of non-realistic boundary conditions in the "S" domain, in particular in terms of heat flux. The solid material volume to fluid volume ratio should be conserved in order to properly represent the heat flux in the equipement. Consequently, the proposed solution is to define, around the curve "C", the three-dimensional channel as a highly radially

conductive fictive solid "S2" [17], as shown in Figure 3. The idea is to transmit in each channel cross section the temperature from “C” to the walls of “S2”, consistently with the cross section averaging of the 1D fluid approach.

The computational domain thus consists of a one-dimensional zigzag channel “C” of total developed length equal to L, where the process fluid flows; a three-dimensional zigzag solid domain “S2” of total developed length equal to L; and a three-dimensional solid bloc “S” surrounding “S2”, which represents the solid material in the heat exchanger/reactor, with a thickness t, width w and length l.

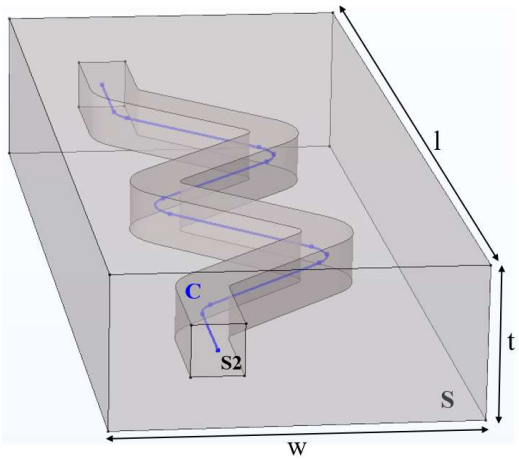


*Figure 3: Illustration of the simulated geometry using the 1D/3D approach.*

A sensitivity study was carried out in order to consistently determine the material properties of “S2” [17]. In order to be able to set the radial thermal conductivity, a curvilinear coordinate system was defined for "S2”. The axial (resp. radial) components of the "S2" thermal conductivity are then set along this curvilinear coordinate system to zero (resp. to $10^5$ $W{\cdot}m^{-1}{\cdot}K^{-1}$) [17].

## 2.3 Model equations

The 1D simulation work is based on the resolution of classical continuity and momentum equations for steady state and an incompressible fluid flowing inside the channel [17]:

$$\rho_p u \cdot \nabla u = -\nabla p_p - \Lambda \frac{\rho_p}{2 d_{h,p}} u|u| \quad (1)$$

$$\nabla \cdot (S_p \rho_p u) = 0 \quad (2)$$

where u is the cross section averaged velocity ($m{\cdot}s^{-1}$), ρ the fluid density ($kg{\cdot}m^{-3}$), p pressure (Pa), Λ (dimensionless) the Darcy friction factor, $d_h$ the mean hydraulic channel diameter (m) and S the channel cross section area available for flow ($m^2$). The subscript p refers to the process side.

The Darcy friction factor Λ is calculated from Théron et al. [16]’s correlation, established for the zigzag millichannel, in function of the Reynolds number $Re_p$ as shown in equation (3). The Reynolds number in the channel is calculated using equation (4), where μ is the fluid viscosity (Pa·s).

$$\Lambda = 24.3 \cdot \mathrm{Re_p^{-0.71}} \text{ for } 20 < \mathrm{Re_p} < 200$$
$$\Lambda = 6 \cdot \mathrm{Re_p^{-0.43}} \text{ for } 200 < \mathrm{Re_p} < 2250 \quad (3)$$

$$\mathrm{Re} = \frac{\rho \cdot u \cdot d_h}{\mu} \quad (4)$$

Let $e_t = (e_{t,x}\ e_{t,y}\ e_{t,z})$ be the unit tangent vector to the channel axis (Figure 4).


*Figure 4: Unit tangent vector to the channel axis.*

The 1D simulation work solves for the tangential velocity $u_p$ that is defined as follows:

$$u = u_p \cdot e_t \quad (5)$$

In addition, the solved energy equation for an incompressible fluid flowing in the channel is the following:

$$\rho_p S_p C_{p,p} u \cdot \nabla T_p = \nabla \cdot S_p \lambda_p \nabla T_p + \Lambda \frac{\rho_p S_p}{2 d_{h,p}} |u|^3 + Q_{wall} \quad (6)$$

Where $T_p$ is the process fluid temperature (K), $\lambda$ is the fluid thermal conductivity ($W \cdot m^{-1} \cdot K^{-1}$), $C_p$ is the heat capacity at constant pressure ($J \cdot kg^{-1} \cdot K^{-1}$) and $Q_{wall}$ represents external heat exchange through the channel wall ($W \cdot m^{-1}$). This radial heat transfer from the surroundings into the channel is given by:

$$Q_{wall} = h_p P_p (T_S - T_p) \quad (7)$$

where P is the wetted perimeter of the channel (m), $h_p$ is the convective heat transfer coefficient ($W \cdot m^{-2} \cdot K^{-1}$) inside the channel and $T_S$ the external temperature outside the channel (K).

$h_p$ is deduced from the Nusselt number correlation (8) established for the zigzag millichannel of the DeanHex heat exchanger/reactor [30] for $550 < Re_p < 8623$. $Pr_p$ is the Prandtl number in the process channel, calculated using equation (9).

$$\mathrm{Nu_p} = \frac{h_p \cdot d_{h,p}}{\lambda_p} = 0.16 \cdot \mathrm{Re_p^{0.66}} \cdot \mathrm{Pr_p^{0.33}} \quad (8)$$

$$\mathrm{Pr} = \frac{C_p \cdot \mu}{\lambda} \quad (9)$$

$T_s$ in equation (7) is given as the temperature field computed in the 3D surrounding solid. In this way, heat transfer coupling is done between 1D channel flow and the 3D side as a line source. In other words, the temperature coupling between the channel and the surrounding domain is implemented as a line heat

source in the 3D domain. The source strength is proportional to the temperature difference (7) between the channel fluid and the surrounding domain.

In this work, in the case of implementing a chemical reaction that takes place in a homogeneous phase, the source term $Q_r$, which is the heat released ($W \cdot m^{-1}$) by the reaction, is added to the energy balance equation (6) and a mass transfer equation (10) is added to the above-mentioned equations resolved by the 1D model, where C and R are the concentration ($mol \cdot m^{-3}$) and the rate of consumption ($mol \cdot m^{-3} \cdot s^{-1}$) of the limiting reactant, respectively.

$$u \cdot \nabla C = R \tag{10}$$

In addition, a heat balance equation is resolved for the 3D surrounding solid, taking into account the conduction in the solid material as well as the convective heat transfer through the solid S walls [17]:

$$\nabla \cdot (-\lambda_S \nabla T_S) = q_S \tag{11}$$

where $\lambda_s$ is the thermal conductivity ($W \cdot m^{-1} \cdot K^{-1}$) of the 3D solid, $T_S$ the solid temperature (K) and $q_S$ the convective heat flux ($W \cdot m^{-2}$) at the solid S walls [17].

The validation of the proposed approach is done by comparing the obtained 1D/3D results, firstly, to 3D CFD calculations, secondly, to experimental results. Finally, in order to show the importance of the 3D solid representation, a sensitivity study about the influence of the solid material thermal conductivity is conducted, as well as a comparison of 1D/3D results to 1D calculations.

## 3. 3D CFD VS 1D/3D SIMULATIONS

### 3.1 Straight channel

In order to validate the proposed 1D/3D approach in the simple case of a straight channel, a comparison is made with a full 3D simulation using ANSYS Fluent CFD code.

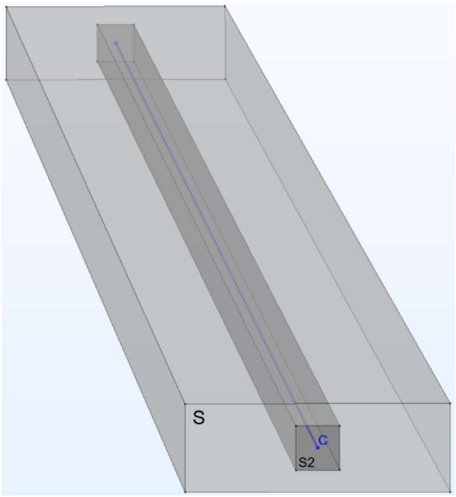


*Figure 5: Schematic of the simulated geometry using the 1D/3D approach for the straight channel configuration.*

**Computational domain and meshing**

The computational domain consists of a square cross-section (2×2 $mm^2$) 1 meter long straight channel, embedded in a parallelepipedic (w=12 mm, t=4 mm and l=1 m) solid matrix. The latter is made of structural steel with a thermal conductivity of 44 $W \cdot m^{-1} \cdot K^{-1}$. The simulated geometry using the 1D/3D approach is shown in Figure 5, where the one-dimensional straight channel is added (which is no more than the pipe axis).

For the 3D CFD simulations, the cross-sectional mesh is made of cells with a typical size of about $3 \times 10^{-4}$ m in the center of the channel which get finer (five cell layers) close to the walls in order to ensure the most accurate resolution at the wall (cf. Figure 6a). The surrounding solid is meshed three times coarser than the center of the fluid. The 3D CFD mesh is thus made of 1 030 000 cells, while in the 1D/3D calculations, it consists of only 60 000 cells (cf. Figure 6, b). Grid independence studies, for both simulations, were conducted to ensure that the solution, in terms of thermal profile, is not influenced by the size of the grid.

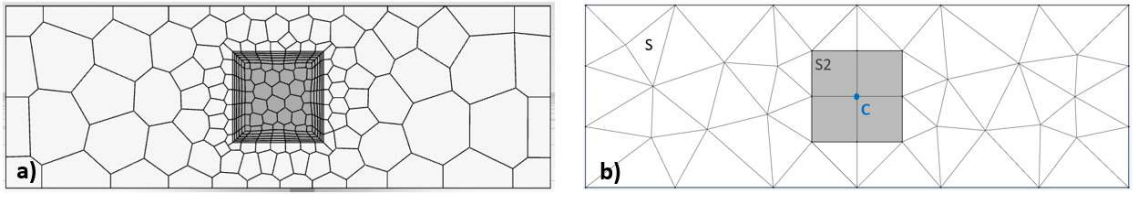


*Figure 6: Illustration of the mesh in the cross-section of the a) 3D CFD and b) 1D/3D simulated geometry.*

**Equations and boundary conditions**

For both simulations, at the channel inlet, constant velocity and temperature conditions are assumed (equal to 0.069 $m \cdot s^{-1}$ and 20 °C respectively). At the channel outlet, an average pressure of 1 atm is set.

The fluid is heated through its passage in the channel due to a constant temperature boundary condition (equal to 60 °C) on the solid external walls.

In the 3D CFD simulations, a no-slip condition is applied to the channel walls and a steady laminar flow is considered. Continuity, momentum (Navier-Stokes) and energy equations for an incompressible fluid are solved. In the 1D/3D model, the following Nusselt correlation [31] (equation (12)) is integrated into the 1D model, where x is the axial coordinate of the channel, in order to take into account the fact that the flow is not established close to the inlet. Note that Nu = 2.98 corresponds to a fully developped laminar flow in channels of square cross-sections, with a uniform temperature boundary condition on the four external channel walls [32].

$$\mathrm{Nu_p} = 2.98 + \frac{\left(0.049 + \frac{0.020}{\mathrm{Pr_p}}\right) \cdot \left(\mathrm{Re_p} \cdot \mathrm{Pr_p} \cdot \frac{\mathrm{d_{h,p}}}{\mathrm{x}}\right)^{1.12}}{1 + 0.065 \cdot \left(\mathrm{Re_p} \cdot \mathrm{Pr_p} \cdot \frac{\mathrm{d_{h,p}}}{\mathrm{x}}\right)^{0.7}} \tag{12}$$

**Results**

The computed temperature field in the 1D/3D calculation corresponds to average temperature values in the channel cross sections, along the channel axis (x-axis). In the 3D CFD calculation, the average temperature at axial location x is calculated, during post-processing, from the computed velocity v ($m \cdot s^{-1}$) and temperature T (K) fields, as follows:

$$\mathrm{T_p} = \frac{\iint \mathrm{T} \cdot \mathrm{v} \cdot \mathrm{da}}{\iint \mathrm{v} \cdot \mathrm{da}} \tag{13}$$

The average temperature profiles for both calculations are represented in Figure 7. It can be observed that the 1D/3D model describes well the heat transfer in the channel. The maximum relative error in temperature between the 1D/3D and 3D CFD simulations is less than 7%, which is acceptable. This difference may result from the use of the above-mentioned Nu correlation (12) in the 1D/3D simulation because the condition of a constant temperature at the walls of the channel is not verified. Instead, it is the temperature at the external walls of the solid S that is fixed in the simulation. Therefore, the Nusselt correlation may introduce an inaccuracy in this simulated case.

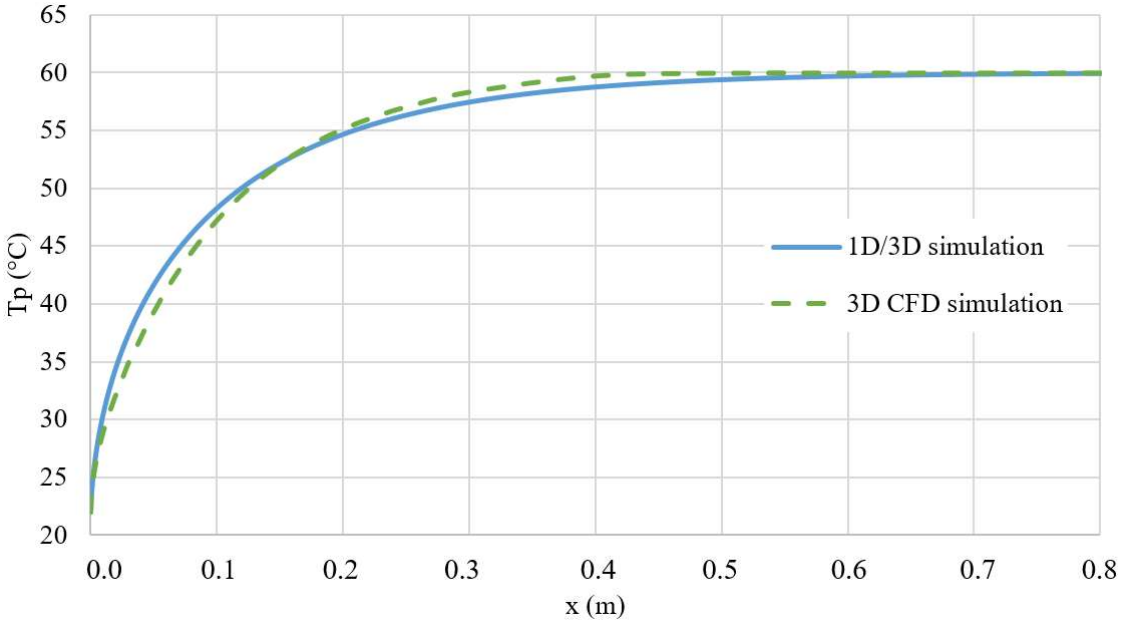


*Figure 7: Comparison between 1D/3D and 3D CFD simulations in terms of mean temperature profile of the fluid for a straight channel.*

## 3.2 Zigzag Channel

To go further, more complexity is added to the model. A corrugated geometry is now considered. It consists of the 2×2 $mm^2$ zigzag channel used by Théron et al. [16]. The 1D/3D simulated thermal profiles are compared to 3D CFD results obtained using the finite volume CFD code ANSYS Fluent 2020 R1.

**Computational domain and meshing**

For the comparison with 3D CFD results, only a part of the 2×2 $mm^2$ zigzag process channel is modelled since the full 3D modelling of the zigzag channel is very expensive in computational resources. The process channel length L is reduced to about 0.1 m, which represents roughly the first row of the original process channel shown in Figure 1, a.

The computational domain consists of a zigzag channel that starts and ends at half a straight section (cf. Figure 8) where the fluid flows in the 3D CFD simulations and the one-dimensional zigzag channel is added (which is no more than the three-dimensional zigzag channel axis) in the 1D/3D simulations; and a zigzag solid matrix (t=w=6 mm and l=0.1 m), surrounding the three-dimensional channel, representing the solid material of the process and closing plates (the utility plates are not modelled). The solid material is the stainless steel with a thermal conductivity of 16.3 $W \cdot m^{-1} \cdot K^{-1}$.

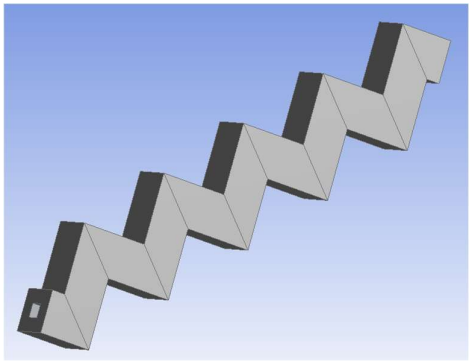

*Figure 8: The modelled portion of the channel in the 1D/3D and 3D CFD simulations.*

For the 3D CFD simulations, in order to provide an efficient and accurate resolution, a refined meshing is constructed for the channel, as shown in Figure 9, a. In the channel cross-section where the fluid flows, the mesh size is $10^{-4}$ m at the center and $2\times10^{-5}$ m near the wall, with five layers. The solid matrix is meshed five times coarser than the center of the fluid. The mesh consists of about six million cells.

For the 1D/3D mesh, a free tetrahedral meshing is applied to the 3D solid domains where only thermal conduction takes place. There is no need for a finely constructed meshing (cf. Figure 9, b). The mesh consists of 205 681 cells. Grid independence studies were conducted to ensure that the solution, in terms of thermal profile, is not influenced by the size of the grid.

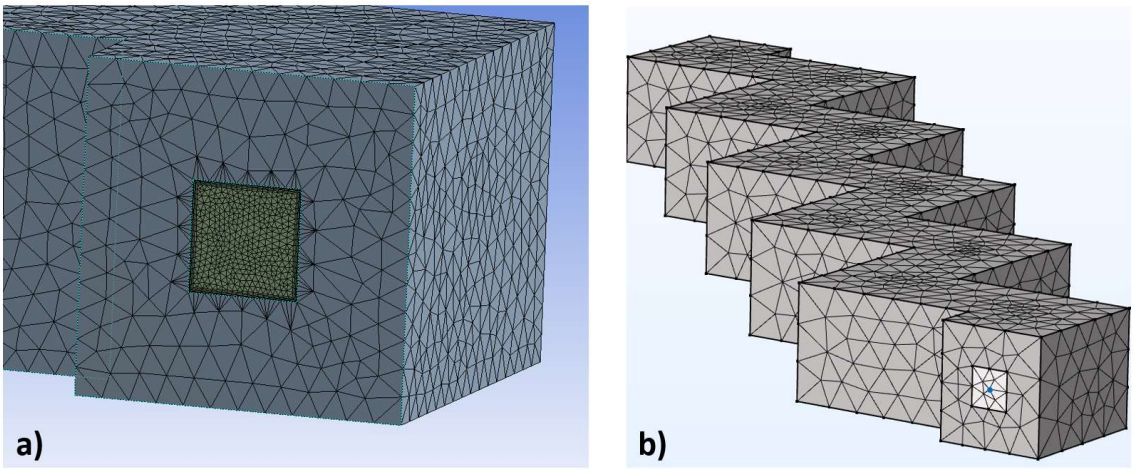


*Figure 9: Illustration of the mesh for the process channel and the surrounding solid used in the a) 3D CFD simulations and b) 1D/3D simulations.*

**Equations and boundary conditions**

For the 3D CFD calculations, the SST k-ω turbulence model is used. In fact, in the simulated cases, the Reynolds number varies between 700 and 2250. Numerical studies in zigzag geometries similar to the one studied in the present work show that the flows can become unsteady at Reynolds number around

500 [29], [33]. All simulations are at steady state. Continuity, momentum (Navier-Stokes) and energy equations for an incompressible fluid are solved.

In a previous work [17], the consistency of the 1D/3D numerical approach for the simulation of heat transfer in the DeanHex was shown by comparison with experimental data from [16]. In the present study, the same conditions are used to compare the two types of simulations (1D/3D vs 3D CFD).These experimental conditions are presented in Table 2. $Q_p$ and $Q_u$ ($kg \cdot h^{-1}$) are the mass flowrates of the process and utility fluids, respectively. Note that the high utility flowrate guarantees that the heat transfer process is not limited by the local heat transfer coefficient on the utility side (the thermal resistance on the utility side is 3 to 6 times lower than that on the process side). At the channel inlet, a constant temperature $T_{p,in}$ (°C) is set. At the outlet, an atmospheric pressure condition is set.

Since the utility channels are not modelled, a heat flux boundary condition "$q_S$" (14) is imposed on the upper and lower external walls of "S" to represent the cooling side. "$q_S$" is equal to zero at the remaining sides of "S". Figure 10, b illustrates this representation in the 1D/3D model.

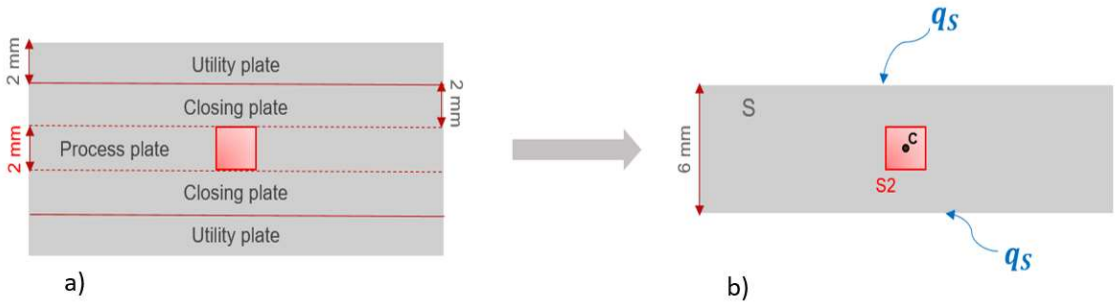


*Figure 10: Schematic of: (a) the plates' configuration in the reactor with a zoom-in on the channel inlet and (b) its representation in the 1D/3D model.*

The heat flux boundary condition "$q_s$" is expressed as follows:

$$q_S = h_u \cdot (T_S - T_u) \cdot \frac{A_u}{A_S} \tag{14}$$

where the subscript u refers to the utility side. $T_u$ is the utility fluid temperature (K). It is assumed uniform and constant along the channels. This hypothesis is confirmed by the inlet and outlet temperature measurements on the utility side in [16] (relative difference less than 4%) where the utility fluid flowrate is 8 to 23 times higher than the process fluid flowrate.

The convective heat transfer coefficient $h_u$ ($W \cdot m^{-2} \cdot K^{-1}$) in the zigzag 2×2 $mm^2$ utility channels, shown in Figure 1, b, is deduced from the following Nusselt correlation [29]:

$$Nu_u = \frac{h_u \cdot d_{h,u}}{\lambda_u} = 0.2 \cdot (Re_u^{0.67} + 8.9) \cdot Pr_u^{0.3} \cdot \left(\frac{d_{h,u}}{L_{s,u}}\right)^{0.4} \tag{15}$$

where $Re_u$ and $Pr_u$ are the Reynolds and Prandtl numbers for the utility side. $d_{h,u}$ and $L_{s,u}$ are, respectively, the hydraulic diameter (m) and the straight length (m) between the bends in the utility

zigzag channels. The physicochemical properties of the utility fluid (water), such as its thermal conductivity $\lambda_u$ ($W \cdot m^{-1} \cdot K^{-1}$), are estimated at $T_u$ (K).

However, when representing the utility channels of heat transfer surface area equal to $A_u$ ($m^2$) by a heat flux boundary condition on the wall of "S" of surface area equal to $A_s$ ($m^2$), a correction factor equal to $\frac{A_u}{A_S}$ should be applied, in order to take into consideration the difference in heat transfer areas [17].

| Utility side | | Process side | | |
|---|---|---|---|---|
| $Q_u$ ($kg \cdot h^{-1}$) | $T_u$ (°C) | $Q_p$ ($kg \cdot h^{-1}$) | $Re_p$ | $T_{p,in}$ (°C) |
| 152 | 15.6 | 2.4 | 554 | 76 |
| | | 4 | 937 | |
| | | 5.5 | 1303 | |
| | | 6.9 | 1641 | |

*Table 2: Operating condition applied for the simulations.*

**Results**

For the 3D CFD simulations, the average temperature in the channel cross section is calculated from the computed temperature and velocity fields using equation (13). The average temperature profiles for both calculations are presented in Figure 11 in function of the channel length. A maximum relative error in temperature of less than 2% highlights a very good agreement between 1D/3D and 3D CFD simulations.

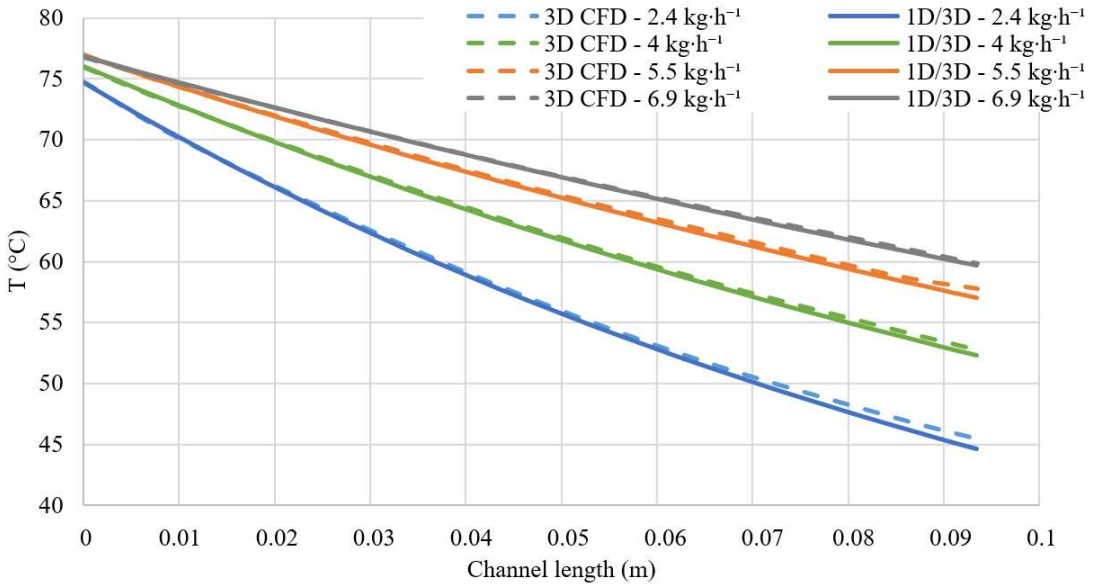


*Figure 11: Evolution of the 1D/3D and 3D CFD simulated process fluid temperature along the process channel for different process flowrates.*

Once the results consistency between 1D/3D and 3D CFD is shown, it is interesting to point out the following observation that highlights the CPU related interest of the 1D/3D model. A 0.1 m long channel requires 6 million cells to be modelled using 3D CFD approach leading to up to 4 hours lasting simulations, whereas only 205 681 cells are used in the 1D/3D simulations that converge in less than 5 min (CPU used: Intel(R) Xeon(R) Silver 4214 CPU @ 2.20GHz  2.19 GHz  (2 processors)). Assuming that the heat transfer correlations are known, the proposed model in this paper allows a significant reduction of computational resources compared to full 3D simulations, which is of interest when it comes to modelling the full-scale heat/exchanger reactor, with a channel total developed length of 6.6 m.

Therefore, based on the comparison between 1D/3D and 3D CFD simulations for the straight and zigzag channels, the performance of the 1D/3D model proves to be acceptable. In the next section, experimental results from Théron et al. [16] are used as a supplementary validation of the proposed approach.

## 4. EXPERIMENTS VS 1D/3D SIMULATIONS

### 4.1 Description of the heat exchanger/reactor used in the experiments

The experimental work of Théron et al. [16] is about a DeanHex reactor at pilot-scale. This HEX reactor is made of stainless steel (thermal conductivity equal to 16.3 $W \cdot m^{-1} \cdot K^{-1}$) and consists of a stack of three process plates (P1, P2 and P3) and four utility plates (U1, U2, U3 and U4), which configuration is represented in Figure 12. 2 mm square cross-section channels, with periodic zigzag units, were engraved on both plates by laser machining (Figure 1). The process and utility plates are sandwiched between 2 mm thick metal plates (closing plates) (Figure 10, a).

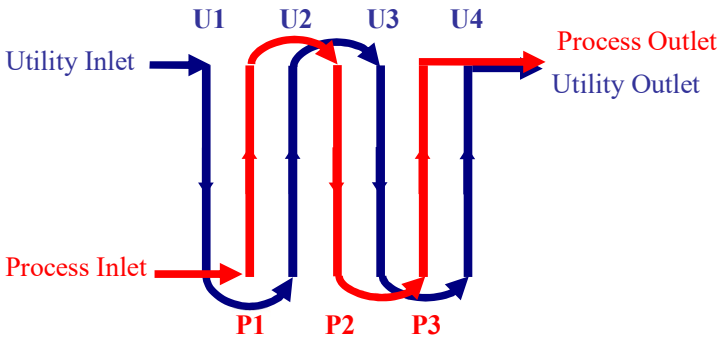


*Figure 12: Process and utility plates configuration in Théron et al. [16]'s pilot.*

In the work of Théron et al. [16], experiments were performed with the implementation of a highly exothermic oxidation reaction. The latter is added in the 1D/3D model and simulations of the heat transfer with chemical reaction are conducted in order to make comparisons with the experimental results and to validate the proposed model.

### 4.2 Computational domain and meshing

The first process plate of 2.2 m long zigzag channel can be modelled as shown in Figure 13 [17], where the configuration "C-S2-S" is established. However, in order to have the same residence time of the reactants into the reactor as in the experiments, the process channel of the whole reactor (6.6 m of total developed length) should be considered. Therefore, three geometries like the one illustrated in Figure 13 are placed in series to have the 6.6 m long channel for the reaction. The free tetrahedral mesh consists of 1 068 720 cells for the 6.6 m long zigzag channel.

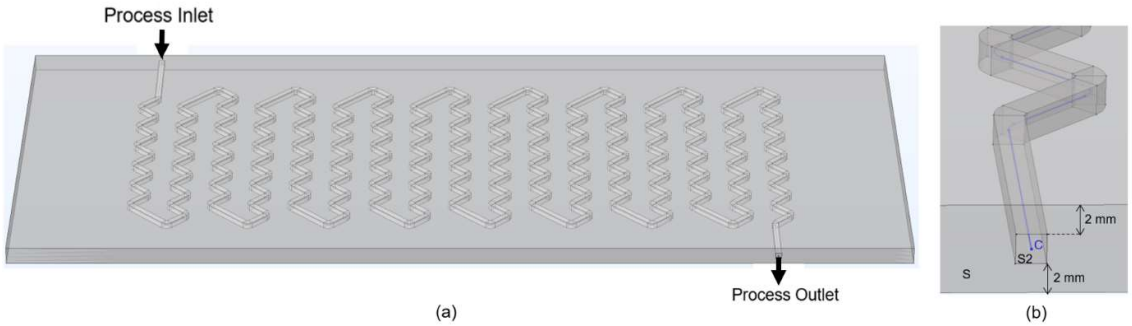


*Figure 13: Illustrations from the 1D/3D model of: (a) the first process plate of Théron et al.[22]'s pilot with the inlet and outlet of the flow and (b) a zoom-in on the process inlet where the C-S2-S chain is showed [17].*

### 4.3 Equations and boundary conditions

For the 1D/3D simulations, the experimental conditions listed in Table 3 are employed. $T_{p,in}$ is applied at the inlet of "C" and an atmospheric pressure at its outlet. The cooling side is represented by a heat flux boundary condition "$q_S$" (14) on the upper and lower walls of the solid S, as described previously. $T_u$ in (14) is equal to the average of the inlet and outlet temperatures of the utility fluid obtained during each experiments and listed in Table 3. Adiabatic boundary conditions are assumed on the other sides of the solid S.

### 4.4 Reaction kinetics

The considered reaction is the oxidation reaction of sodium thiosulfate ($Na_2S_2O_3$) by hydrogen peroxyde ($H_2O_2$) which is written:

$$2Na_2S_2O_3 + 4H_2O_2 \rightarrow Na_2S_3O_6 + Na_2SO_4 + 4H_2O$$

For this first order reaction with respect to both reactants, the reaction rate "r" is expressed as a function of the reactants' concentrations, as follows:

$$r = k \cdot C_{Na_2S_2O_3} \cdot C_{H_2O_2} \quad (16)$$

where the kinetic constant k is assumed to be governed by an Arrhenius law, as follows:

$$k = k_0 \cdot e^{-E_a/\mathcal{R}\cdot T_p} \quad (17)$$

The kinetic parameters of equation (17), obtained by Grau et al. [34] ($k_0$=8.13 × $10^8$ $m^3 \cdot mol^{-1} \cdot s^{-1}$, $E_a/\mathscr{R}$=9156 K) are used in the simulations, since they best fit the experimental results of Théron et al. [16]. The reaction takes place in a homogeneous liquid phase, therefore the mixture fluid properties and total process flowrates are considered in the 1D model. The consumption rate of the limiting reactant R in equation (10) is $R_{Na_2S_2O_3} = -2r$. The 1D model solves the mass balance equation for $C_{Na_2S_2O_3}$. Thus, $C_{H_2O_2}$ is replaced by the following expression that is deduced from the mass balance in the reactor, taking into consideration the stoechiometric coefficients of the reaction:

$$C_{H_2O_2} = C_{H_2O_2,in} - 2 \cdot \left(C_{Na_2S_2O_3,in} - C_{Na_2S_2O_3}\right) \quad (18)$$

where $C_{Na_2S_2O_3,in}$ and $C_{H_2O_2,in}$ are the concentrations of sodium thiosulfate and hydrogen peroxide ($mol.m^{-3}$) at the reactor inlet.

This irriversible and fast reaction is highly exothermic with a heat of reaction $\Delta H_r$=-586.2 $kJ \cdot mol^{-1}$ of $Na_2S_2O_3$. The heat generated ($W \cdot m^{-1}$) during the reaction, integrated in the 1D model, is thus equal to:

$$Q_r = R_{Na_2S_2O_3} \cdot \Delta H_r \cdot S_p \quad (19)$$

Where $S_p$ ($m^2$) is the cross section of the channel.

| N° Exp. | Utility side | | | Process side | | | | |
|---|---|---|---|---|---|---|---|---|
| | $Q_u$ ($kg \cdot h^{-1}$) | $T_{u,in}$ (°C) | $T_{u,out}$ (°C) | $Q_p$ ($kg \cdot h^{-1}$) | $Re_p$ | $T_{p,in}$ (°C) | $C_{Na_2S_2O_3,in}$ ($mol.m^{-3}$) | $C_{H_2O_2,in}$ ($mol.m^{-3}$) |
| 1 | 113 | 39.7 | 39.9 | 14 | 2481 | 17.6 | 378 | 889 |
| 2 | 113.5 | 39.7 | 40.4 | 5 | 879 | 19.3 | 375 | 900 |
| 3 | 113 | 39.7 | 41.1 | 7 | 1266 | 20.0 | 382 | 870 |
| 4 | 112 | 49.6 | 50.7 | 7 | 1378 | 20.7 | | |
| 5 | 112.5 | 59.4 | 60.1 | 7 | 1498 | 21.1 | | |

*Table 3: Experimental conditions for simulating the heat exchange with chemical reaction.*

### 4.5 Results

Since in the experiments the high utility flowrate guarantees that the heat transfer process is not limited by the local heat transfer coefficient on the utility side (the thermal resistance on the utility side is 3 to 6 times lower than that on the process side), the comparison of the experimental results with the 1D/3D simulation results will show the effect of the proposed approach on the process side. Therefore, referring to Théron et al. [16]'s experiments for the validation of the 1D/3D approach is suitable.

The simulated and experimental results are compared in terms of outlet process temperature and conversion rate, as shown in Table 4. The maximum relative difference in outlet process temperature ($\frac{T_{p,out,simu}-T_{p,out,exp}}{T_{p,out,exp}}$) is less than 8%, which is acceptable.

Since hydrogen peroxide is in excess during the reaction, the conversion rate obtained in the simulations is calculated according to the concentration loss of sodium thiosulfate. Théron et al. [16] have calculated the conversion rate using two different methods:

- Reactor: based on a thermal balance between the inlets and outlets of the process and utility streams at steady state;
- Dewar: based on measuring the adiabatic temperature rise in the Dewar vessel from the sampling until reaching the equilibrium temperature.

Both methods induce some errors in the calculation of the rate of conversion of the sodium thiosulfate. The differences in temperature, used in the thermal balance, between the inlet and outlet of the utility fluid (cf. Table 3) may fall in the experimental error of the temperature measurements and thus the conversion rate calculated thanks to the first method may be inaccurate. This may justify the differences in conversion rate obtained in the simulations compared to the experimental "reactor" conversions, especially in experiment n°1 where $T_{u,out}$-$T_{u,in}$=0.2°C. Regardless this experiment, the relative difference in conversion ($\frac{Conversion_{simu}-Conversio\ _{reactor}}{Conversion_{reactor}}$) is less than 12%.

Furthermore, the sampling time in the Dewar method may not be negligible in comparison with the residence time of the reactants in the reactor, which will lead to an overestimation of the conversion rate at the reactor outlet, as seen in Table 4 when comparing simulated to experimental "Dewar" conversions. Nevertheless, the relative difference in conversion ($\frac{|Conversion_{simu}-Conversion_{Dewar}|}{Conversion_{Dewar}}$) is less than 5%.

Overall, in terms of outlet process temperature and conversion rates, the simulations seem to succeed in reproducing the experimental results. Therefore, it could be deduced that the 1D/3D model with the radially infinite thermal conductivity imposed for "S2" proposed in this work is valid for the DeanHex reactor considering these experimental data.

| N° Exp. | Théron et al. [16] | | | Simulation (this work) | | Residence time (s) |
|---|---|---|---|---|---|---|
| | $T_{p,out,exp}$ (°C) | Conversion | | $T_{p,out,simu}$ (°C) | Conversion | |
| | | Reactor | Dewar | | | |
| 1 | 43.9 | 60 | 59 | 40.6 | 73 | 6.9 |
| 2 | 41.4 | 82 | 94 | 40.2 | 92 | 19.3 |
| 3 | 43.4 | 88 | 91 | 40.7 | 86 | 13.8 |
| 4 | 51.0 | 93 | 100 | 50.3 | 96 | 13.8 |

| | | | | | | |
|---|---|---|---|---|---|---|
| 5 | 59.2 | 95 | 100 | 59.8 | 99 | 13.8 |

*Table 4: Comparison between simulated and experimental results for the reaction of sodium thiosulfate oxidation by hydrogen peroxide.*

It is also interesting to visualize the temperature distribution in the solid material of the reactor plate, which is one of the assets of the proposed model in particular when comparing to 1D classical models. This is done for a cut plane that corresponds to an orthogonal 2D coordinate system embedded in the 3D geometry. This plan passes through the middle of the fictive solid "S2". The temperature distribution obtained when simulating experiment n°4 (Table 3) is illustrated in Figure 14.

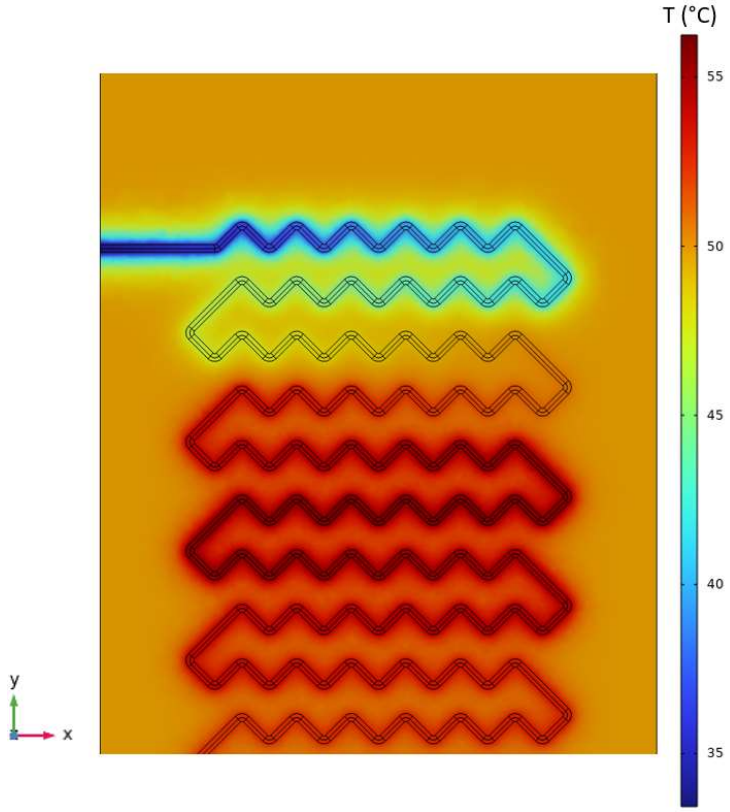


*Figure 14: Temperature distribution in the solid material corresponding to experiment n°4.*

The solid temperature varies with the process fluid temperature which is plotted in Figure 15 (SS plot). The reactants enter the channel at 20.7°C and are heated by the utility side ($T_u$=50.1°C) and by the heat generated by the occurring reaction. The process temperature increases gradually and reaches 60°C. Then, it decreases towards $T_u$ due to the cooling effect of the utility side. This temperature variation is observed in Figure 14 from the solid perspective. Furthermore, temperature gradients are observed between adjacent channels. Far from the process channel, the solid temperature is close to the utility temperature.

In the next section, the actual influence of the conjugate heat transfer on the thermal performances of the heat exchanger/reactor is discussed.

# 5. INFLUENCE OF CONJUGATE HEAT TRANSFER

## 5.1 Sensitivity study about the solid material conductivity

In order to better understand the influence of conjugate heat transfer in the case of millistructured heat exchanger/reactors, a sensitivity study about the influence of the solid material thermal conductivity has been conducted. Therefore, a negligible thermal conductivity (0.01 $W \cdot m^{-1} \cdot K^{-1}$) is tested to simulate the case without heat transfer between channels and three other typical values of material conductivities for an intensified heat exchanger: glass (1 $W \cdot m^{-1} \cdot K^{-1}$), stainless steel (16.3 $W \cdot m^{-1} \cdot K^{-1}$) and silicon carbide (170 $W \cdot m^{-1} \cdot K^{-1}$).

In the previously described simulated case (section 4), the reactor solid material is stainless steel. Hence, the obtained results when simulating the experiment n°4 (Table 3) are used in the sensitivity study for the stainless steel case. Considering the same conditions, new simulations are done by only changing the thermal conductivity of the solid material to 0.01; 1 and 170 $W \cdot m^{-1} \cdot K^{-1}$. Four temperature and conversion profiles are shown in Figure 15 to demonstrate the influence of solid material conductivities on the thermal behaviour of the reactor. Simulated fluid temperatures are plotted as lines over the channel length and reaction conversions are shown as symbols. When increasing the conductivity of the solid, the temperature inside the channel is better controlled. The heat generated by the chemical reaction is dissipated in the solid and the temperature peak is reduced. Whereas in the case of an insulator, the process temperature is out-of-control and continues to increase as shown in Figure 15. In addition, the reaction kinetics depend on the process temperature (equation (17)), thus the effect of the solid conductivity is also observed on the obtained conversions. This highlights the effects of heat conduction in the solid material on the heat exchanger/reactor performances.

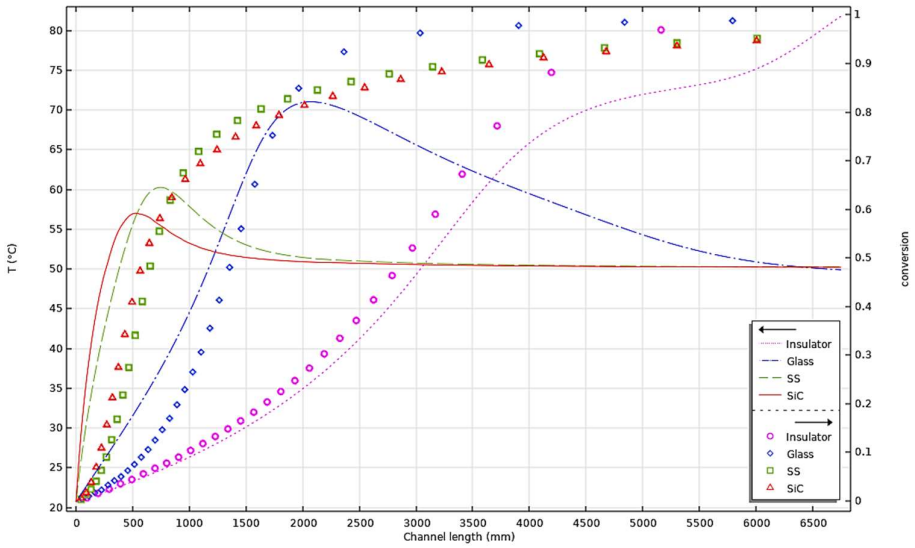


*Figure 15: Thermal profile (lines) and reaction conversion (symbols) in the channel for different plate solid materials.*

In addition, in terms of heat flux distribution in the solid material, Figure 16 shows the y-axis component of the conductive heat flux for the SiC case on the cut plane that passes through the middle of the fictive solid "S2". This y-axis component of the heat flux illustrates the heat flow between adjacent channels.

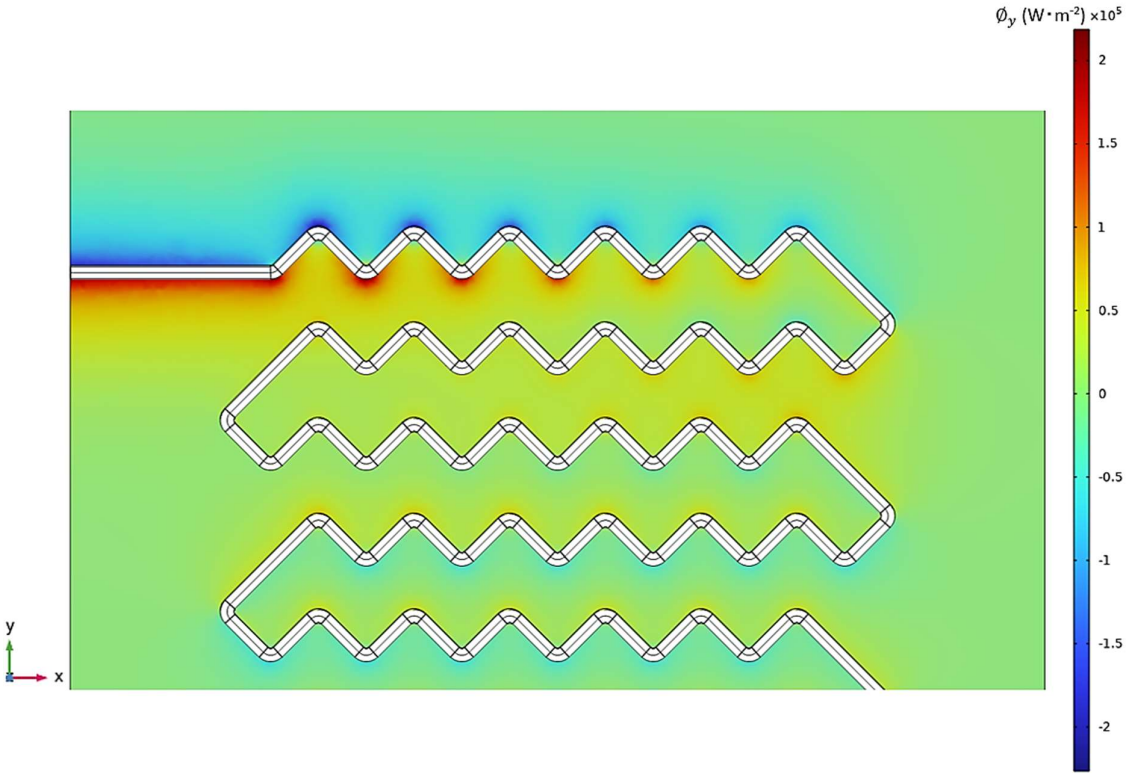


*Figure 16: Y-axis component of the conductive heat flux distribution in the solid material corresponding to experiment n°4.*

This heat conduction flux between adjacent channels is indeed clearly observed, especially between channel rows 1-2 and 2-3. This flow magnitude may reach $0.5\times10^5$ to $2\times10^5$ W·m$^{-2}$ and hence, it is not negligible.

## 5.2 Comparison with the 1D classical model results

A temperature profile is calculated assuming a one-dimensional heat flow between utility and process channels and is then compared to the temperature profile of the 1D/3D model.

Basic heat transfer without chemical reaction is considered. Therefore, on the one hand, the first process plate of the "DeanHex" is simulated using the 1D/3D model by applying the conditions listed in Table 2 ($Q_p$=6.9 L·h$^{-1}$). On the other hand, based on a 1D classical plug-flow model, a temperature profile is calculated from the energy balance over an element dl (m) of the process channel length (equation (20)).

$$\frac{dT_p}{dl} = \frac{4 \cdot \left(\frac{1}{h_p} + \frac{1}{h_u} + \frac{e}{\lambda_S}\right)^{-1} \cdot (T_p - T_u)}{Q_p \cdot C_{p,p}} \qquad (20)$$

Where e (m) is the solid thickness between process and utility plates.

The obtained thermal profiles are shown in Figure 17.

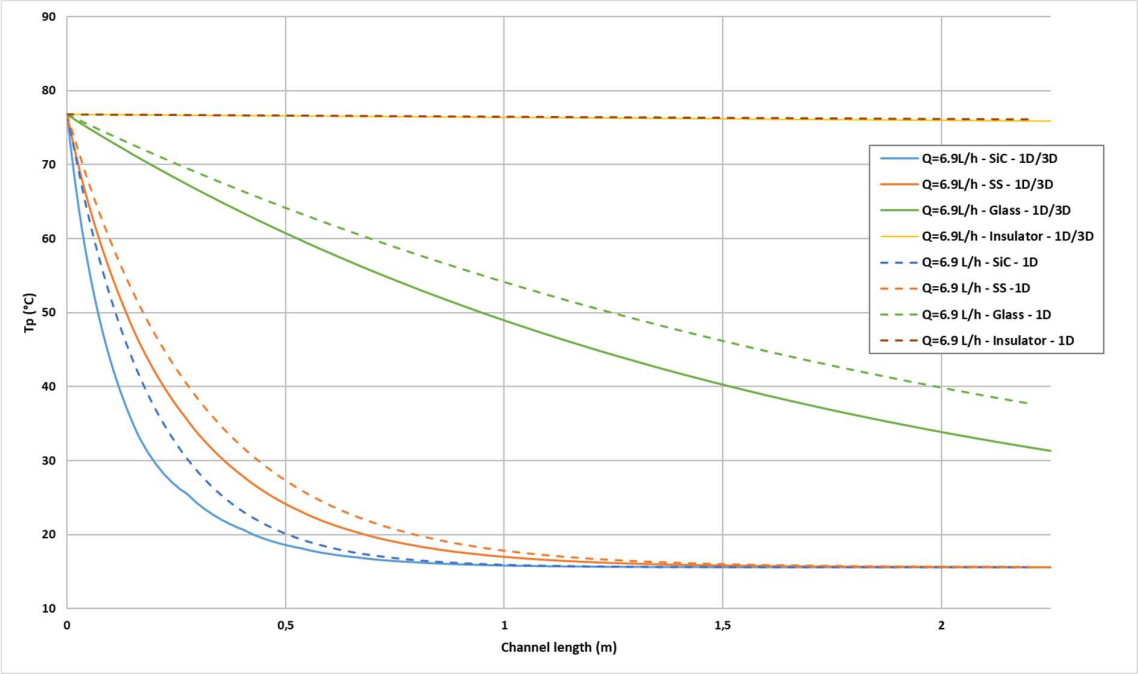


*Figure 17: 1D/3D vs 1D process temperature profiles along the channel length for different solid materials.*

Differences between both temperature profiles are observed for each tested solid material. This shows that the heat is not only transported from the process fluid perpendicularly through the wall to the utility fluid as it is the case with 1D calculations. Axial heat conduction effects exist and are taken into account in the 1D/3D model. When decreasing the conductivity of the solid material to nearly 0, these effects are less significant and thus the 1D/3D and 1D temperature profiles match better. This result shows once again the effect of the conduction in the solid material of the heat exchanger/reactor and justifies the idea of this work that is to take into account the axial heat conduction in the channel walls.

## 6. CONCLUSIONS

This paper deals with a new 1D/3D numerical approach proposed in order to model the DeanHex reactor at a reasonable CPU cost despite the complexity of the channel geometry and its high $L/d_h$ ratio. The model is based on the coupling of a 1D representation of the flow channel with a 3D surrounding solid. In this way, the solid to fluid volume ratio in the reactor is conserved and the heat transfer process is well simulated, especially when implementing extremely high exothermic chemical reactions. Firstly, the heat exchange without chemical reaction has been investigated in the DeanHex reactor using the 1D/3D model. The consequent simulated thermal profiles have been firstly compared to 3D CFD simulations (less than 2% relative difference and significant computational time reduction (5min vs 4h)). Secondly, a highly exothermic reaction was implemented and the simulated results were compared to experimental ones in terms of outlet temperature (less than 8% relative difference) and conversion rates (less than 12% relative difference). The proposed model provides a precise computation of the conversion rate from the concentration loss of reactants, which is a crucial parameter for the reactor.

Based on these comparisons, the 1D/3D approach has proved to be promising and valid for the DeanHex reactor. Furthermore, the effect of conjuguate heat transfer is investigated by comparing 1D/3D results to 1D calculations and by conducting a sensitivity study about the thermal conductivity of the solid material. Both investigations showed the presence of conjugate heat transfer in heat flows between adjacent channels and their influence on the millistructured heat exchanger/reactor performances. These results highlight the importance of taking into account the conduction effects in the solid material of the reactor in the numerical model. Moreover, assuming the availability of heat transfer and friction laws, either from experiments or from dedicated validated 3D CFD calculations on a restricted number of periodic units, the 1D/3D model could be used for other corrugated channels, usually with high $L/d_h$ and solid volume to fluid volume ratios, exchanging heat in all directions with the surrounding medium. Other reactions that occur in a homogeneous phase can also be modelled using the approach described in this paper. The next step is thus to extend the use of this model for two-phase flows (heterogeneous reactions and mass transfer limitations) as well as in dynamic mode to evaluate the effects of operating condition deviations on reaction control regarding the material thermal capacitance. At the end, the aim is to build a generalized scaling-up model for the purpose of predicting, at industrial scale, the performance of the heat exchanger/reactor in terms of conversion rate and energy efficiency.

## ACKNOWLEDGEMENTS

This research did not receive any specific grant from funding agencies in the public, commercial, or not-for-profit sectors.

## NOMENCLATURE

$S$ cross-sectional area ($m^2$)

$A$ heat exchange area ($m^2$)

$C_p$ specific heat of the fluid ($J \cdot kg^{-1} \cdot K^{-1}$)

$d_h$ hydraulic diameter (m)

$t$ thickness of solid matrix (m)

$l$ solid matrix length (m)

$w$ solid matrix width (m)

$e$ solid thickness between process and utility plates (m)

$\Lambda$ Darcy friction factor

$h$ heat transfer coefficient ($W \cdot m^{-2} \cdot K^{-1}$)

$L$ channel developed length (m)

$L_s$ straight section length (m)

$Q$ volumetric flow rate ($m^3 \cdot s^{-1}$)

$Nu$ local Nusselt number

$Pr$ Prandtl number

$q$ heat flux ($W \cdot m^{-2}$)

$R_c$ radius of curvature (m)

$Re$ Reynolds number

$T$ temperature (K)

$v$ velocity vector ($m \cdot s^{-1}$)

$u$ cross-section mean fluid velocity ($m \cdot s^{-1}$)

$u_p$ tangential velocity ($m \cdot s^{-1}$)

$Q_r$ heat generated by the reaction ($W \cdot m^{-1}$)

$C$ concentration of the reactant ($mol \cdot m^{-3}$)

$r$ reaction rate ($mol.m^{-3}.s^{-1}$)

$R$ consumption rate of the reactant ($mol.m^{-3}.s^{-1}$)

$Ea$ activation energy ($J \cdot mol^{-1}$)

$k$ reaction rate constant ($m3 \cdot mol^{-1} \cdot s^{-1}$)

$k_0$ specific rate constant ($m^3 \cdot mol^{-1} \cdot s^{-1}$)

$\mathcal{R}$ universal gas constant ($J \cdot mol^{-1} \cdot K^{-1}$)

$da$ element of cross-sectional area ($m^2$)

$x$ coordinate over the channel length (m)

$y$ coordinate over the channel width (m)

$z$ coordinate over the channel depth (m)

$e_t$ unit tangent vector

### Abreviations

$Na_2S_2O_3$ sodium thiosulfate

$H_2O_2$ hydrogen peroxide

$Na_2SO_4$ sodium sulfate

$H_2O$ water

*1D* one-dimensional

*2D* two-dimensional

*3D* three-dimensional

*CFD* computational fluid dynamics

### Greek symbols

$\Theta$ angle between two straight sections (°)

$\lambda$ thermal conductivity ($W \cdot m^{-1} \cdot K^{-1}$)

$\mu$ dynamic viscosity ($Pa \cdot s$)

$\rho$ fluid density ($kg \cdot m^{-3}$)

$\Delta H_r$ heat of reaction ($kJ \cdot mol^{-1}$)

### Subscripts

*p* process side

*u* utility side

*s* solid matrix

*in* channel inlet

*out* channel outlet

$Na_2S_2O_3$ relative to the reactant sodium thiosulfate

$H_2O_2$ relative to the reactant hydrogen peroxide

*simu* relative to simulation

*exp* relative to experiment

## REFERENCES


[1] D. Fernandez Rivas *et al.*, 'Process intensification education contributes to sustainable development goals. Part 1', *Education for Chemical Engineers*, vol. 32, pp. 1–14, Jul. 2020, doi: 10.1016/j.ece.2020.04.003.

[2] A. Stankiewicz and J. Moulijn, 'Process Intensification: Transforming Chemical Engineering', *Chemical Engineering Progress*, pp. 22–34, 2000.

[3] T. Van Gerven and A. Stankiewicz, 'Structure, Energy, Synergy, Time - The Fundamentals of Process Intensification', *Ind. Eng. Chem. Res.*, vol. 48, no. 5, pp. 2465–2474, Mar. 2009, doi: 10.1021/ie801501y.

[4] Z. Anxionnaz, M. Cabassud, C. Gourdon, and P. Tochon, 'Heat exchanger/reactors (HEX reactors): Concepts, technologies: State-of-the-art', *Chemical Engineering and Processing: Process Intensification*, vol. 47, no. 12, pp. 2029–2050, Nov. 2008, doi: 10.1016/j.cep.2008.06.012.

[5] I. Nastase and F. Bode, 'Impinging jets – a short review on strategies for heat transfer enhancement', *E3S Web Conf.*, vol. 32, p. 01013, 2018, doi: 10.1051/e3sconf/20183201013.

[6] A. Ghanem, C. Habchi, T. Lemenand, D. Della Valle, and H. Peerhossaini, 'Energy efficiency in process industry – High-efficiency vortex (HEV) multifunctional heat exchanger', *Renewable Energy*, vol. 56, pp. 96–104, Aug. 2013, doi: 10.1016/j.renene.2012.09.024.

[7] Z. Li *et al.*, 'A flapping vortex generator for heat transfer enhancement in a rectangular airside fin', *International Journal of Heat and Mass Transfer*, vol. 118, pp. 1340–1356, Mar. 2018, doi: 10.1016/j.ijheatmasstransfer.2017.11.067.

[8] Z. Anxionnaz-Minvielle, M. Cabassud, C. Gourdon, and P. Tochon, 'Influence of the meandering channel geometry on the thermo-hydraulic performances of an intensified heat exchanger/reactor', *Chemical Engineering and Processing: Process Intensification*, pp. 67–80, Nov. 2013.

[9] A. Rave, R. Kuwertz, G. Fieg, and J. Heck, 'Characterization of a Modular, Scalable Millistructured Plate Reactor', *Chemie Ingenieur Technik*, vol. 91, no. 5, pp. 602–606, May 2019, doi: 10.1002/cite.201800203.

[10] S. Schwolow, A. Neumüller, L. Abahmane, N. Kockmann, and T. Röder, 'Design and application of a millistructured heat exchanger reactor for an energy-efficient process', *Chemical Engineering and Processing: Process Intensification*, vol. 108, pp. 109–116, Oct. 2016, doi: 10.1016/j.cep.2016.07.017.

[11] K.-J. Wu, V. Nappo, and S. Kuhn, 'Hydrodynamic Study of Single- and Two-Phase Flow in an Advanced-Flow Reactor', *Ind. Eng. Chem. Res.*, vol. 54, no. 30, pp. 7554–7564, Aug. 2015, doi: 10.1021/acs.iecr.5b01444.

[12] C. Phillips and K. Symonds, 'Development of a novel integrated chemical reactor-heat exchanger', *BHR Group Conf. Ser. Publ.*, vol. 38, pp. 71–87, 1999.

[13] E. Mielke *et al.*, 'Micro-reactor mixing unit interspacing for fast liquid-liquid reactions leading to a generalized scale-up methodology', *Chemical Engineering Journal*, vol. 352, pp. 682–694, Nov. 2018, doi: 10.1016/j.cej.2018.07.043.

[14] L. Prat *et al.*, 'Performance Evaluation of a Novel Concept "Open Plate Reactor" Applied to Highly Exothermic Reactions', *Chemical Engineering & Technology*, vol. 28, no. 9, 2005, doi: 10.1002/ceat.200500120.

[15] S. Schwolow, B. Mutsch, N. Kockmann, and T. Röder, 'Model-based scale-up and reactor design for solvent-free synthesis of an ionic liquid in a millistructured flow reactor', *Reaction Chemistry & Engineering*, vol. 4, no. 3, pp. 523–536, 2019, doi: 10.1039/C8RE00148K.

[16] F. Théron, Z. Anxionnaz-Minvielle, M. Cabassud, C. Gourdon, and P. Tochon, 'Characterization of the performances of an innovative heat-exchanger/reactor', *Chemical Engineering and Processing: Process Intensification*, vol. 82, pp. 30–41, Aug. 2014, doi: 10.1016/j.cep.2014.04.005.

[17] A. Maarawi, Z. Anxionnaz-Minvielle, P. Coste, N. Di Miceli Raimondi, and M. Cabassud, '1D/3D Numerical Approach for Modelling a Milli-Structured Heat Exchanger/Reactor', *Chemical Engineering Transactions*, vol. 86, pp. 1441–1446, Jun. 2021, doi: 10.3303/CET2186241.

[18] E. B. Nauman, *Chemical Reactor Design, Optimization, and Scaleup*. Hoboken, NJ, USA: John Wiley & Sons, Inc., 2008. doi: 10.1002/9780470282076.

[19] A. Rave, R. Kuwertz, G. Fieg, and J. Heck, 'Modeling and experimental investigation of the spatial heat transfer in a plate reactor with meandering millichannels', *Chemical Engineering and Processing - Process Intensification*, vol. 150, p. 107860, Apr. 2020, doi: 10.1016/j.cep.2020.107860.
[20] Z. Dai, D. F. Fletcher, and B. S. Haynes, 'Impact of tortuous geometry on laminar flow heat transfer in microchannels', *International Journal of Heat and Mass Transfer*, vol. 83, pp. 382–398, Apr. 2015, doi: 10.1016/j.ijheatmasstransfer.2014.12.019.
[21] S. Premkumar D, P. Swaminadhan, and B. Sreedhara Rao, 'Optimization of corrugation angle for the heat transfer performance of corrugated plate heat exchangers', *International Research Journal of Engineering and Technology*, vol. 3, no. 7, pp. 924–929, Jul. 2016.
[22] N. R. Rosaguti, D. F. Fletcher, and B. S. Haynes, 'Low-Reynolds number heat transfer enhancement in sinusoidal channels', *Chemical Engineering Science*, vol. 62, no. 3, pp. 694–702, Feb. 2007, doi: 10.1016/j.ces.2006.09.045.
[23] Z. Zheng, D. F. Fletcher, and B. S. Haynes, 'Laminar heat transfer simulations for periodic zigzag semicircular channels: Chaotic advection and geometric effects', *International Journal of Heat and Mass Transfer*, vol. 62, pp. 391–401, Jul. 2013, doi: 10.1016/j.ijheatmasstransfer.2013.02.073.
[24] Z. Zheng, D. F. Fletcher, and B. S. Haynes, 'Chaotic advection in steady laminar heat transfer simulations: Periodic zigzag channels with square cross-sections', *International Journal of Heat and Mass Transfer*, no. 57, pp. 274–284, 2013.
[25] J. Facão and A. C. Oliveira, 'Modeling Laminar Heat Transfer in a Curved Rectangular Duct with a Computational Fluid Dynamics Code', *Numerical Heat Transfer, Part A: Applications*, vol. 48, no. 2, pp. 165–177, Jul. 2005, doi: 10.1080/10407780590948918.
[26] Y. Sui, C. J. Teo, and P. S. Lee, 'Direct numerical simulation of fluid flow and heat transfer in periodic wavy channels with rectangular cross-sections', *International Journal of Heat and Mass Transfer*, vol. 55, no. 1–3, pp. 73–88, Jan. 2012, doi: 10.1016/j.ijheatmasstransfer.2011.08.041.
[27] C. M. Karale, S. S. Bhagwat, and V. V. Ranade, 'Flow and heat transfer in serpentine channels', *AIChE J*, vol. 59, no. 5, pp. 1814–1827, May 2013, doi: 10.1002/aic.13954.
[28] W. M. Abed, R. D. Whalley, D. J. C. Dennis, and R. J. Poole, 'Numerical and experimental investigation of heat transfer and fluid flow characteristics in a micro-scale serpentine channel', *International Journal of Heat and Mass Transfer*, vol. 88, pp. 790–802, Sep. 2015, doi: 10.1016/j.ijheatmasstransfer.2015.04.062.
[29] H. Shi, N. Di Miceli Raimondi, D. F. Fletcher, M. Cabassud, and C. Gourdon, 'Numerical study of heat transfer in square millimetric zigzag channels in the laminar flow regime', *Chemical Engineering and Processing - Process Intensification*, vol. 144, p. 107624, Oct. 2019, doi: 10.1016/j.cep.2019.107624.
[30] Z. Anxionnaz *et al.*, 'RAPIC project: Toward competitive heat-exchanger/reactors', *The 3rd European Process Intensification Conference (EPIC)*, Manchester, UK, Jun. 20, 2011.
[31] G. Nellis and S. A. Klein, *Heat transfer*. Cambridge ; New York: Cambridge University Press, 2009.
[32] R. K. Shah and A. L. London, 'Rectangular Ducts', in *Laminar Flow Forced Convection in Ducts*, Elsevier, 1978, pp. 196–222. doi: 10.1016/B978-0-12-020051-1.50012-7.
[33] Z. Zheng, D. F. Fletcher, and B. S. Haynes, 'Transient laminar heat transfer simulations in periodic zigzag channels', *International Journal of Heat and Mass Transfer*, vol. 71, pp. 758–768, Apr. 2014, doi: 10.1016/j.ijheatmasstransfer.2013.12.056.
[34] M. D. Grau, J. M. Nougués, and L. Puigjaner, 'Batch and semibatch reactor performance for an exothermic reaction', *Chemical Engineering and Processing: Process Intensification*, vol. 39, no. 2, pp. 141–148, Mar. 2000, doi: 10.1016/S0255-2701(99)00015-X.